XMM-Newton

XMM-Newton Science Analysis System 8.0 scientific validation

XMM-SOC-USR-TN-0017 Issue 1.0

C.Gabriel, A.Ibarra, R.González-Riestra, M.Guainazzi, A.Pollock,
R.Saxton, M.Stuhlinger, A.Talavera
XMM-Newton Science Operations Centre

S.Rosen, M.Sakano
XMM-Newton Science Survey Centre

1 October 2008

Revision history

Revision number	Date	Revision author	Comments
0.1	14 April 2008	C. Gabriel	Test plan for SASv8.0
0.9	27 August 2008	C. Gabriel	Draft Public version for SASv8.0
1.0	1 October 2008	C. Gabriel	Public version for SASv8.0

Contents

1 Introduction

1.1 Concept

Scientific Validation (SV) is required in order to ensure a constant high quality of the XMM-Newton Science Analysis System (SAS).
The main purpose of the SV is to provide the SAS community with a stable reliable software product, as well as to generate a list of caveats and known deficiencies. Together with these "functional" tests, the SV provides some information on the expected systematic uncertainties when basic data analysis products are generated through the current version of the SAS, using the best calibrations available at the moment SAS was released. It is important to stress that *this document does not supersede or substitute* the **instrument calibration status documents**, available from the XMM-Newton calibration portal. Instrument calibration is a continuous activity, whose results (update of calibration files) is intrinsically and necessarily decoupled from software releases. XMM-Newton users are recommended to consult periodically the URL: `http://xmm.esac.esa.int/external/xmm_sw_cal/calib`, which informs on the calibration status of the XMM-Newton instruments.
The document you are reading (*SAS Science Validation Report*) contains information about:

- which instrumental modes are fully supported by SAS,
- which scientific products SAS can produce,
- the level of accuracy associated with those products,
- a list of caveats and problems.

The SV is performed on a standard set of XMM-Newton observations, which cover all commissioned observational modes, and a number of observations, specially chosen for testing new / special aspects of the data reduction corresponding to the version to be validated. Tab. 1 lists all the datasets used for the validation of SAS version 8.0. Some of these observations are particularly suitable to test calibration-related items, as specified in the rightmost column of Tab. 1. These datasets are partly intended as a standard reference, which has been and will be used to verify the performances of all SAS versions. However, additional datasets may occasionally be used to test version-specific SAS items. This is the case, for instance, for the datasets discussed in Sect. 2 of this report. Datasets discussed in a given report and not listed in Tab. 1 do not belong to the reference datasets, and are therefore not intended to be discussed in later SAS versions validation reports.

1.2 Methodology

The SV for SAS v8.0 consisted of the following steps:

1. the same datasets are also processed through the SAS reduction meta-tasks: `e[mp]proc`, `om[ifg]chain`, `rgsproc`
2. products generated by the above steps are used as basis for the *interactive SV analysis*. Standard scientific products (images, light curves, spectra, source lists) are generated and analyzed. This allows to:
   - test the SAS interactive tasks.

Table 1: SV datasets

Instrument	Mode	Object	Revolution Obs. ID	ID	Calibration item
EPIC MOS	Full Frame	Lockman Hole	544 0147511601	1	Astrometry + source detection
	"	G21.5.09	060 0122700101	2	Effective area
	Small Window (W2)	Mkn 421	165 0099280201	3	
	Large Window (W3)	PKS0558-504	153 0129360201	4	Effective area
	Timing Uncompressed	Her X-1	207 0134120101	5	Timing
EPIC-pn	Full Frame	Lockman Hole	544 0147511601	1	Astrometry
	Full Frame/Small Window	PKS0558-504	153 0129360201	4	Effective area
	Large Window	AB Dor	185 0133120201	6	
	Small Window	PKS0558-504	084 0125110101	7	Effective area
	Fast Timing	Her X-1	207 0134120101	5	Timing
		Crab	698 0160960201	8	
	Fast Burst	Crab	411 0153750301	9	Timing
		Crab	411 0153750501	10	Timing
	Extended Full Frame	G21.5-0.9	060 0122700101	2	Effective area
RGS	SPEC+Q	PKS0558-504	084 0125110101	7	
"		Mkn 421	165 0099280201	3	Effective area
	"	AB Dor	185 0133120201	6	Wavelength scale
	"	AB Dor	338 0134521301	11	Wavelength scale
	"	AB Dor	462 0134521601	12	Wavelength scale
	"	AB Dor	572 0134522201	13	Wavelength scale
OM	Image Mode	BPM 16274	261 0125320701	14	Photometry
	Fast Mode	X1822-371	228 0111230101	15	
	FF Low Resolution	BPM 16274	261 0125320701	14	Astrometry
	Optical grism	Hz2	503 0125910901	16	Wavelength scale & flux calibration
	UV Grism	HD13499 (offset)	657 0125911301	17	Wavelength scale & flux calibration

- verify the calibration accuracy obtained with SAS v8.0, and compare it with the expected accuracy on the basis of the calibration status at the time the SV is performed.

The conclusions of the SV are to be summarized in Sect. 8. A list of instrument modes supported by SAS v8.0 reported in Appendix A. A summary of SAS v8.0 capabilities detailed in Appendix B.
In this report: best-fit parameter uncertainties are at the 90% confidence level for 1 interesting parameter ($\Delta\chi^2 = 2.71$); errors on positions or count rates are at the 1-σ level; energies are quoted in the observer's reference frame unless otherwise specified.

2 New in SAS 8

There are several new elements in SAS 8 with respect to former versions. They can consist of new tasks, or new analysis methods within already existing tasks. All of them have to be scientifically validated, in addition to their standard integration tests.

2.1 New task for light curves background subtraction and exposure correction

The SAS task performing background subtraction and exposure correction of light curves in versions previous to SAS v8.0, `lccorr`, presented several problems, and had to be taken out of the distribution a couple of times. A new alternative task has been developed, named `epiclccorr`. Several observations of Cataclysmic Variables are mainly used for validation. A comparison with the corrected RGS derived light curves by the brighter ones is also part of the test. This should help to validate also the task `rgslccorr`, introduced in SAS v7.1 and only tested functionally so far.

2.2 Slew data analysis fully integrated in SAS

A new metatask performing slew data reduction has been introduced in SAS v8.0: `eslewchain`. It consists of a perl script doing the same data reduction as performed by the Slew Data Processing Software (SDPS) package (v.2.1) distributed so far as a separate package. Now this data reduction has been fully integrated into SAS. The first XMM-Newton slew catalogue XMMSL1 represents the validation of this specific data reduction. Therefore a simple comparison between the results obtained with `eslewchain` to the ones obtained by SDPS should be sufficient. We have chosen the slews 9138800002, 9145000003 and 9099000003 due to the number of sources present in those fields.

2.3 New task for rate dependent CTI and gain correction on PN fast modes

The corrections performed by the new task `epfast` have been tested, using the EPIC PN observations in fast modes (Timing and Burst mode) of the SV standard data set.

2.4 Validation of new strategy against "Time Jumps" in PN data

The changes introduced to the OAL for the new strategy get tested. The default value ("22"), as recommended by the EPIC Calibration Team is tested against different numbers provided via the environment variable "SAS_TIME_JUMP".

2.5 Source detection with SAS 8 - 2XMM and more

Source detection by XMM-Newton data has been considerably improved in the last 2 years, also motivated by the 2XMM source catalogue made public by the SSC Consortium, the largest ever produced X-ray source catalogue. All the improvements included in the 2XMM in this respect had been already introduced in the SAS v7.0. Validation of several aspects of source detection are included in this exercise by comparison of a single observation (with many individual detectable sources) against the 2XMM catalogue. Astrometry, but also detection (mis-)efficiency and aspects of effective area calibration can be tested in this case. The chosen observation is 0147511601, a Lockman Hole observation performed in revolution 544. Combined in this analysis, an evaluation of the (elliptical) 2D PSF approximation for effective area correction was performed, an alternative introduced in SAS v8.0. It is expected that the elliptical PSF approximation can be more accurate for establishing the encircled energy. However, the level of calibration is still to be improved. This can be tested by flux comparisons of the large number of sources included in this field.

2.6 RGS alternative analysis based on a wavelength grid

So far, the data reduction of RGS data has been performed on a grid defined in bins of dispersion angle (Beta). A change in the approach has been requested, basing the analysis on a grid defined in bins of wavelength. This makes possible the rigorous adding of spectra obtained in different observations. In SAS v8.0 we add this possibility yet as an alternative, non default, for performing the data reduction. Since this upgrade implies changes in many tasks of the reduction chain, we consider as necessary collecting experience, before deciding this to be the default reduction way. All of the RGS data included in the general validation exercise (specific for RGS) are both ways reduced and compared. As main test and to show the new capability in its full power, all the observations performed corresponding to following sources are reduced and added together: PKS2155-304 and AB-Dor. The list of observations processed is the following: PKS2155-304: 0124930101, 0124930201, 0124930301, 0124930501, 0124930601, 0080940101, 0080940301, 0080940401, 0080940501, 0158960101, 015896[09-11]01, 015896[10-11]01, 015896[13-15]01, 041178[01-02]01.

AB-Dor: 012372[02-03]01, 0126130201, 0133120201, 0134520301, 0134520701, 013452[13-18]01, 013452[20-29]01, 0160363001.

3 Standard Results:

All the datasets have been succesfully completely reduced, without any exception, by the standard reduction procedures. These are based on the SAS metatasks emproc, epproc, rgsproc, omichain, omfchain and omgchain. Except in a few cases, which require specific parameters for rgsproc (source is not on axis in some of the observations, and therefore the specific coordinates have to be included), this has been done using pure default parameters.
In addition, the whole calibration database has been processed through the standard cross-calibration procedures, which are also based on the SAS metatasks mentioned above, but comprise also spectral model fitting.

3.1 Calibration database processing

The calibration database comprises several hundred observations, of all types of X-ray sources, as observed by XMM-Newton. They are continuously used for cross calibration of the XMM-Newton instruments, but also for cross calibration with instruments from other missions, eg. Chandra and Suzaku. Whenever a new SAS version is to become public, or whenever substantial calibration updates are to be released, data reduction including model fitting takes place of all of the database, or of relevant parts of it.
SAS 8.0 has been used with the standard calibration set, as of July 2008, for reducing 138 observations performed with the X-ray instruments, and model fitting of the corresponding spectra with appropriate models for the source type. There was not a single failure in the processing, and all the results will be public, once review has been completed, under the XMM-Newton Cross Calibration page (http://xmm2.esac.esa.int/external/xmm_sw_cal/calib/cross_cal/).
An example for the product of the cross-calibration is given in Fig. 1, showing the combined spectral fit of an observation of Markarian 421, which is also present in the SV datasets.
Full discussion of the results and conclusions from the cross calibration will also be available in the (updated for SAS 8.0) cross calibration document to be published soon. We can here advance that the quality of spectral fitting is in general just slightly improved with respect to the previous public SAS version and its associated calibration files. Cross-calibration among the instruments shows also slight improvements in several areas.

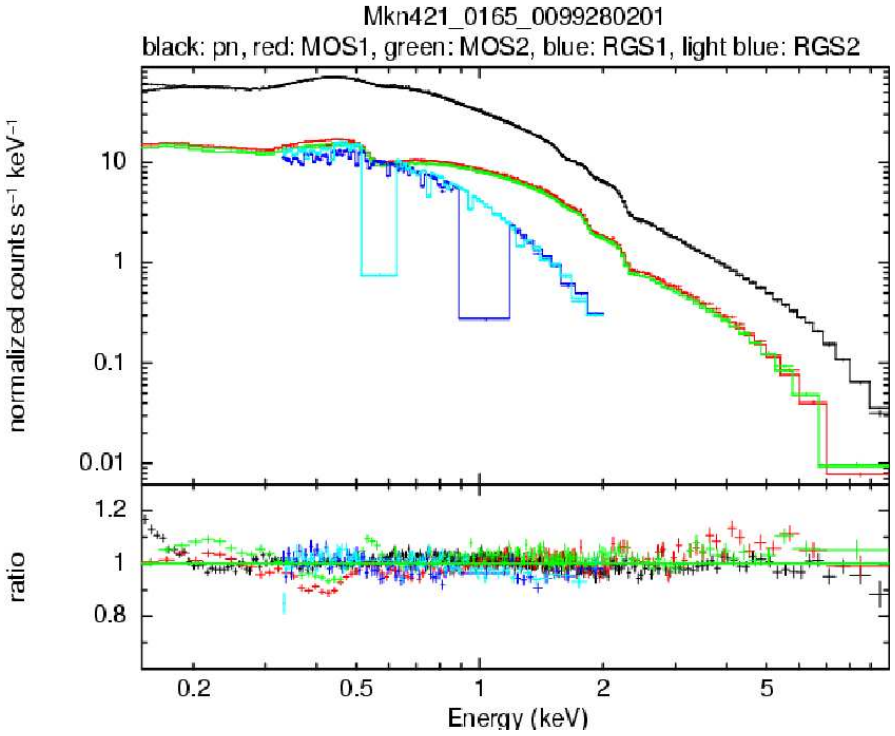

Figure 1: Spectra and residuals of Mkn421 simultaneous (PN, MOS1, MOS2, RGS1 and RGS2) fitting, as performed by the cross calibration tools.

Table 2: Best-fit parameters and results when a photoelectrically absorbed power-law model is applied to the EPIC spectra of G21.5-0.9

Camera	N_H (10^{22} cm^{-2})	Γ	2-10 keV flux (10^{-11} cgs)
MOS1	2.188 ± 0.041	1.854 ± 0.027	6.18 ± 0.05
MOS2	2.202 ± 0.041	1.910 ± 0.027	5.97 ± 0.05
pn	2.06 ± 0.03	1.824 ± 0.015	6.29 ± 0.03

4 EPIC specific results:

4.1 EPIC camera imaging modes

4.1.1 EPIC cameras effective area: G21.5-09

The X-ray spectrum of the Crab-like SuperNova Remnant (SNR) G21.5-0.9 (Warwick et al. 2001) is well described by a strongly absorbed (column density, $N_H \sim 2 \times 10^{22}$ cm^{-2}) power-law. At 0-th order, it can be characterized through 3 quantities only: N_H, the photon index Γ and the model normalization or flux. This source is therefore particularly well-suited to compare the performances of the response matrices above 1 keV.
The XMM-Newton observation discussed in this report was performed on April 7, 2000. The EPIC cameras were operating in Full Frame (MOS), and Extended Full Frame (pn) mode, respectively. The source was on-axis. Data were reduced with the `procs` EPIC reduction meta-tasks.
Source spectra were extracted from circular regions of $2.7'$ radius around the centroid of the SNR. Background spectra were extracted from annuli of $3.15'$ to $4.6'$ radius. The source spectra were rebinned in order to have at least 50 counts in each spectral bin and to oversample the instrumental energy resolution by a factor not higher than 3. The spectra were fit in the 0.5-10 keV and 0.3-10 keV energy bands for MOS and p-n, respectively. Effective areas were generated using exposure-specific detector maps, as recommended for extended sources. As already stressed in former Science Validation Reports, wrong results are obtained, if one uses a *flat* detector map in either `arfgen` or `rmfgen`.
The best-fit results are shown in Tab. 2 and Fig. 2, and Fig. 3. Residuals are within $\pm 5\%$ across the whole sensitive bandpass of the EPIC cameras. The MOS 2 cameras exhibits a steeper spectrum ($\Delta\Gamma \lesssim 0.05$), and a lower 2–10 keV flux by $\simeq 4\%$.
In the Γ versus N_H plane (see Fig. 3), the pn iso-$\chi 2$ contour are now no longer consistent with the MOS ones (cf. Fig.1 in the SASv6.5 Science Validation Report). This is, however, entirely due to calibrations. In particular, this larger discrepancy is due to a combination of a change in the MOS redistribution (from version `43` to version `65` of the `EMOS?_REDIST` CCF constituents, occurred on November 22, 2005; such a change is applicable to all epochs earlier than July 15, 2000), increasing the column density measured by the MOS cameras by $\simeq 4 \times 10^{20}$ cm^{-2}; and of an update of the pn high-energy effective area (from version `10` to version `11` of the `XRT3_XAREAEFF` CCF constituent, occurred on April 7, 2007), making the pn spectrum flatter by $\simeq 0.02$ (a later change to the long-term CTI correction introduces another marginal change in the overall spectral shape). For a more detailed and comprehensive discussion of the cross-calibration status among the EPIC cameras, readers should refer to http://xmm2.esac.esa.int/external/xmm_sw_cal/calib/cross_cal/.

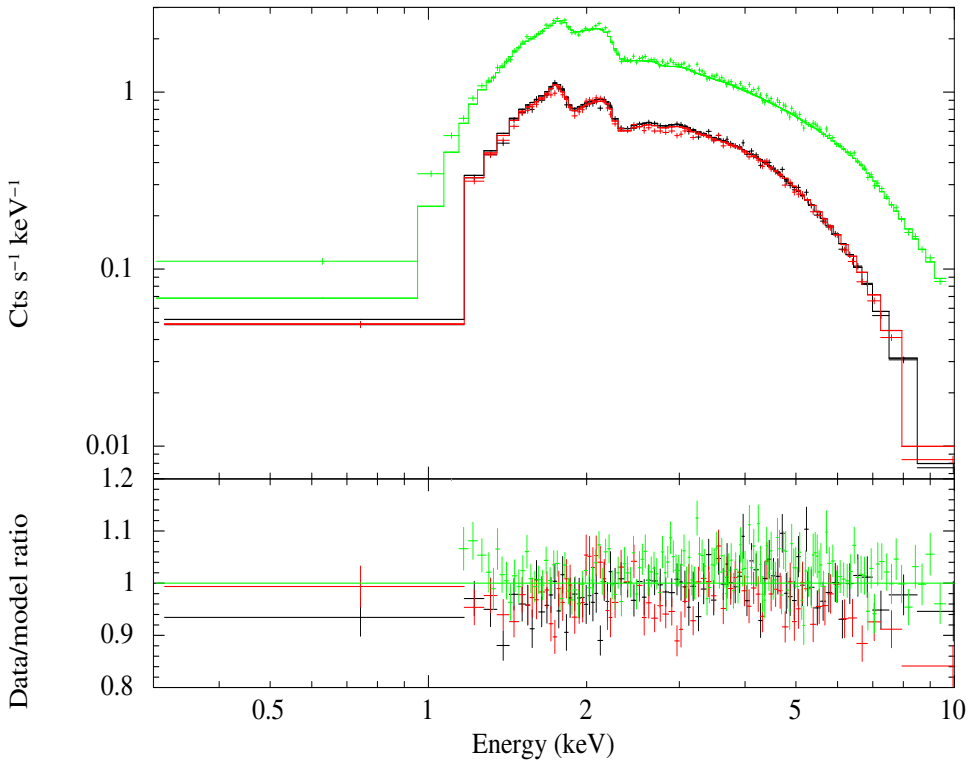

Figure 2: EPIC spectra (*upper panel*) and residuals in units of data/model ratio (*lower panel*), for the spectral fit in Tab. 2; MOS1: *black*; MOS 2: *red*; pn *green*. Each data point corresponds to a signal-to-noise ratio $\geq$25.

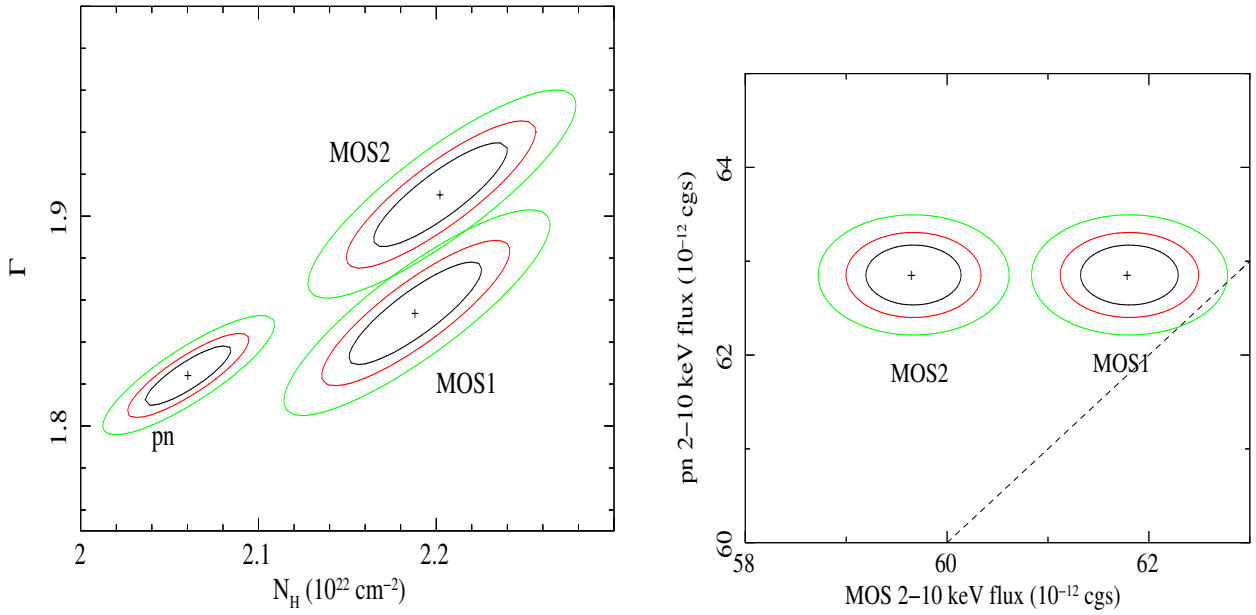

Figure 3: *Left panel*: iso-χ^2 contour plots for N_H versus Γ. Contours are at 68%, 90%, and 99% confidence levels for two interesting parameters. *Right panel*: iso-χ^2 contour plots for the MOS 2–10 keV observed flux versus the pn flux in the same energy band. The *dashed line* indicates the locus of equal fluxes

4.2 EPIC-pn fast modes

4.2.1 Her-X1–Validation of EPIC-pn Timing mode

XMM-Newton observed Her-X1 ($\alpha_{2000} = 16^h57^m49^s.80$, $\delta_{2000} = +35°20'32''.6$), several times. The observation used in this report took place on January 26, 2001, Rev.#207, lasting more than 9000 seconds.
For this analysis only EPIC-pn data have been used. We used the following setting to extract source and background regions, respectively: `((RAWX,RAWY) IN box(36.5,100,25,99.5,0))`, `((RAWX,RAWY) IN box(5,100.75,4.5,99.25,0))`. Spectra have texibeen extracted using single and double events neglecting the events at CCD borders and events lower than 0.5 keV where data should not be used due to the high noise below 0.5 keV in EPIC-pn Timing Mode.
All response files have been created using SAS 8.0. The spectra have been fit with a model constituted by photoelectric absorption (the `wabs` implementation in XSPEC was used), a power-law, a disk blackbody, and four Gaussian lines (two of them intrinsically broad). Several residual features are known to be due to current uncertainties in the calibration. Fig. 4 shows a plot of Her-X1 (data and model) of the best fit to the EPIC-pn Timing mode spectrum. The best-fit parameters and results are summarized in Tab. 3.

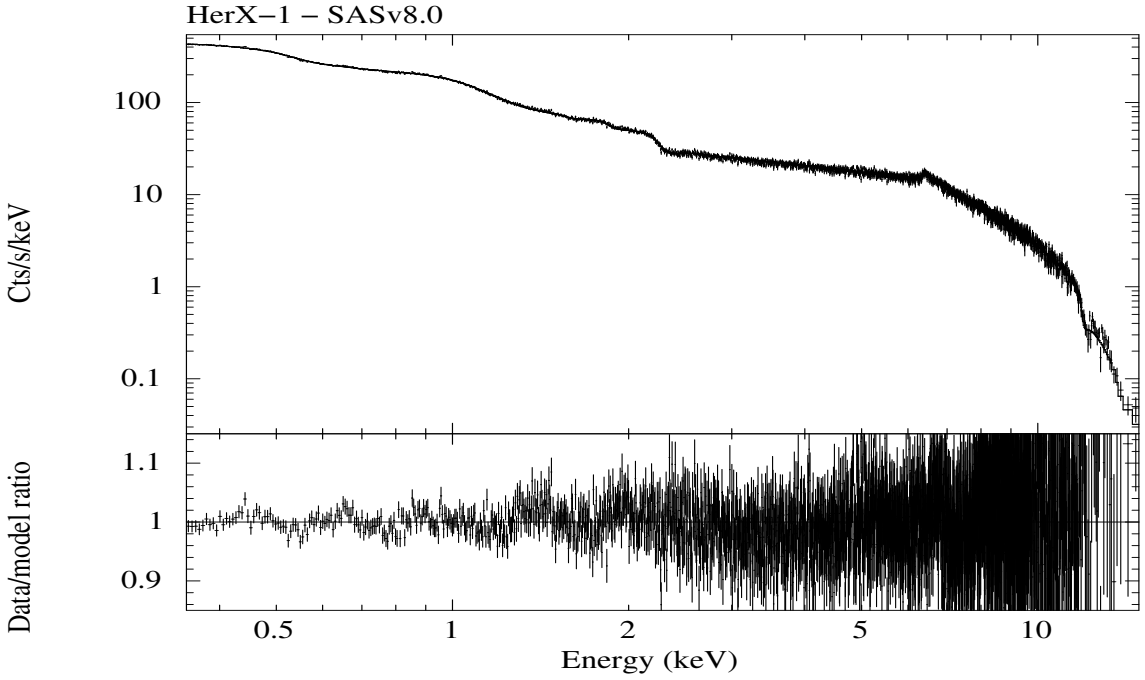

Figure 4: Spectrum of Her-X1 in EPIC pn Timing mode

Table 3: Her-X1 best-fit parameters. The 0.5 keV Gaussian and the sigma of one iron line have been frozen. E_i^C indicates the centroid energy of the i-th line, σ_i its intrinsic width

χ^2/ dof	Γ	Tin	N_{BB}	E_1^C	σ_1	E_2^C	σ_2
		[eV]	[10^4]	[keV]	[keV]	[keV]	[keV]
2515.5/2075	$0.881\pm^{0.007}_{0.005}$	127 ± 6	$8.5\pm^{2.6}_{0.5}$	$0.5^{\dagger}$	$0.005^{\dagger}$	0.904 ± 0.006	$0.184\pm^{0.006}_{0.005}$
				E_3^C	σ_3	E_4^C	σ_4
				[keV]	[keV]	[keV]	[keV]
				$6.44\pm^{0.010}_{0.12}$	$0.005^{\dagger}$	$6.67\pm^{0.05}_{0.04}$	$0.005^{\dagger}$

†frozen

5 RGS specific results

5.1 General comments on SAS RGS data processing

No problems were found in the data reduction, which was performed through both alternative ways: the default by `rgsproc`, with a grid defined in bins of the dispersion angle β, and the new implemented one, basing the analysis on a grid defined in bins of wavelengths. Moreover, comparison of the final results yields a fully consistent picture, despite the method used. The use of this analysis method has been implemented in SAS 8 for making possible the rigorous co-addition of data from different exposures, from RGS1 and RGS2 and different orders. Fig. 5 shows RGS1 and RGS2 first order spectra as derived using the grid in bins of wavelength (in black), each of them overplotted (in red) with the corresponding spectra as derived using the traditional beta grid, zoomed in, for a better judgement.

5.2 The new λ-based spectra of AB Dor in comparison with their β-based versions

While the main objective of providing so-called λ-based spectra accumulated in physical units on a fixed wavelength grid as opposed to instrumental units of dispersion angle of the default β-based spectra was to facilitate the combination of two or more spectra from different observations, it is a clear condition that λ-based spectra from individual observations should be equally reliable for routine analysis. Among the most complex data available to the RGS are the line-rich thermal spectra of active stars. An important part of RGS calibration efforts is the comparison of measured line wavelengths with laboratory values. As part of the verification process, β-based and λ-based spectra were derived for 17 observations of AB Dor for analysis with calibration methods that use a model of an absorbed thermal continuum and 153 narrow lines of known laboratory wavelength. The best-fit fluxes and wavelengths of the $17 \times 153 = 2601$ were determined from the `XSPEC` maximum-likelihood models of the λ-spectra and β-spectra.
Fig. 6 shows the fractional difference $(f_\lambda - f_\beta)/(f_\lambda + f_\beta)$ as a function of f_β: the difference generally amounts to less than a few percent.
Similarly, the comparison of $\Delta\lambda$, the mean shift of the observed line wavelengths from laboratory values in Fig 7 shows agreement between λ values and β values to generally better than 1 or 2 m$\mathring{A}$.

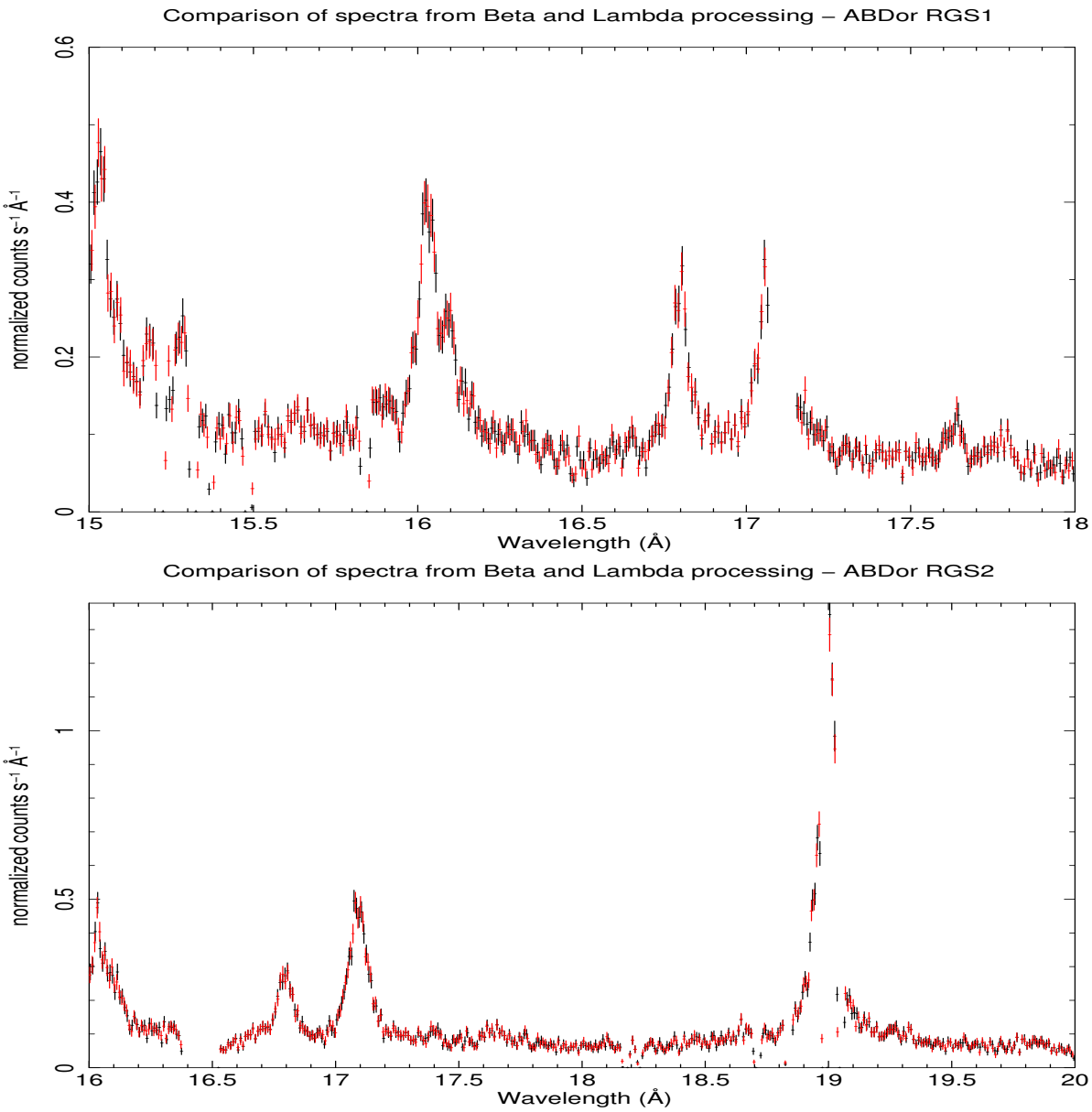

Figure 5: *Upper panel*: RGS1 spectra (zoomed in) derived using the grid in bins of wavelength (in black) vs the spectra obtained using the grid in bins of dispersion angle Beta (in red). *Bottom panel*: Same for RGS2

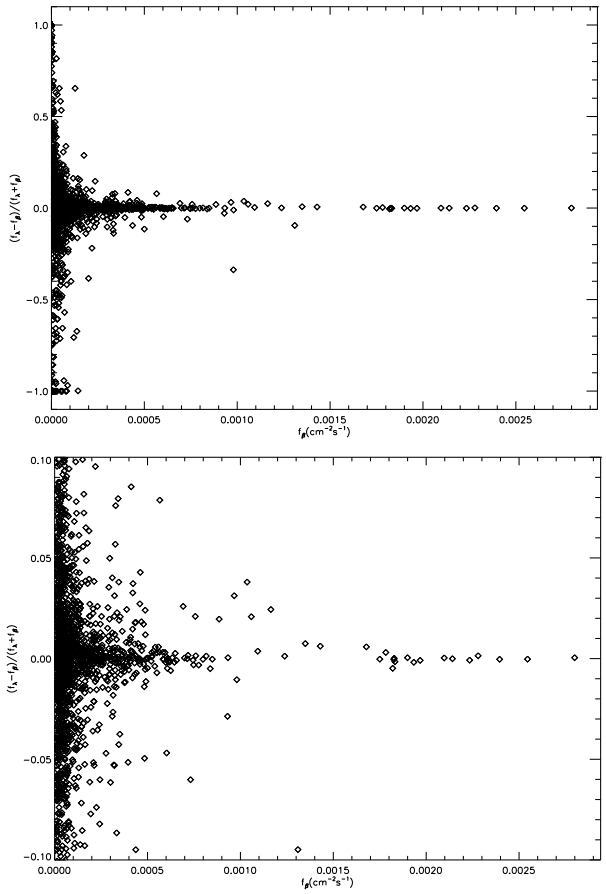

Figure 6: Comparison of 2601 line fluxes measued in spectra of AB Dor accumulated in the two methods offered by SAS v8.0. The values f_β refer to fluxes calculated with spectra accumulated in intervals of the dispersion angle, β and f_λ with spectra accumulated in wavelength, λ, with more details shown in the lower plot.

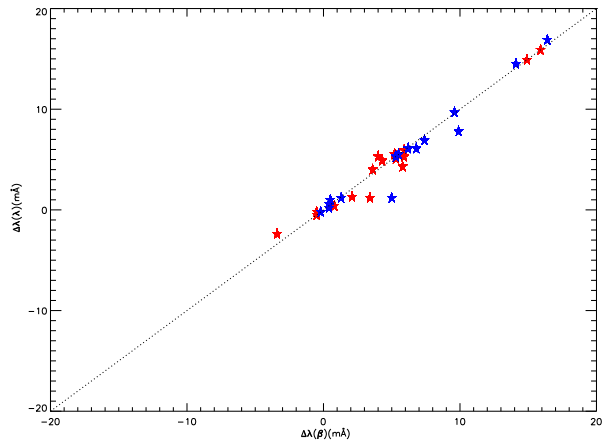

Figure 7: Comparison of the mean wavelength shift, $\Delta\lambda$, from laboratory values of all 153 narrow lines in the model spectrum of AB Dor fitted to spectra accumulated in dispersion angle, β, and wavelength, λ.

6 OM specific results

6.1 General comments on SAS OM data processing

OM calibration and data processing have evolved considerably along the life of SAS until the release of SAS 6.5 that included all aspects of the calibration and a stable configuration with respect to processing algorithms. Newer versions, as the current SAS 8.0, include improvements of the code to make it more robust, particularly in the source detection area, also to correct bugs and some new minor implementations.
In this Science validation, we deal with some of these new aspects. A more extended analysis can be found in the SAS 6.5 science validation.

6.2 SAS OM grism data processing

The detection and matching of zero and first orders has been improved.
A change worth to mention in OM grisms processing is the computation of sky coordinates for all sources in the field of view of the grisms (all zero orders even if their spectrum cannot be extracted - field spectroscopy). For this an additional distortion map for the grism has been created and included in the OM_ASTROMET_0011.CCF. A new image output file with astronomical coordinates (WCS) is created and a sky aligned image is created as well. Although the results are rather satisfactory, this computation has still to be refined.
A new output product of `omgchain` facilitates the checking of the spectral extraction by the user: an image plot with overimposed regions for the zero and first orders is now produced by the `omgrismplot` task.
The interactive extraction of the spectra with `omgsource`, has been made more robust with respect to the previous version.

6.2.1 Field spectroscopy: HD 13499

HD 13499 is a F5V star. It has been observed several times as wavelength calibrator. In the field of view, there is also HD 13434 (F7V). This observation has been performed by off-setting the main target so as to have the spectra of both stars in a full frame low resolution exposure. Only the UV grism has been used, because both stars are too bright for the Visible grism.
`omgchain` has been run in field spectroscopy mode. Fig.8 shows the spectral image with superimposed regions for checking the accuracy of the extraction. Fig.9 shows the sky aligned image that allows the user to now the coordinates of all sources in the f.o.v. This are two of the new products mentioned above.
Now `omgrism` extracts correctly the spectrum of the two stars. Figures 10 and 11 show their extracted net spectra and background in count-rate versus wavelength. The Mg II absorption line at 2800 $\mathring{A}$ is clearly visible. This feature appears shifted for HD 13499. This is due to a slight offset in the determination of the zero order position. This can be improved by interactive extraction using `omgsource`.

6.3 Interactive SAS for OM: a new task

In addition to `omsource` and `omgsource` described and validated for SAS 6.5, a new interactive task is present in SAS 8.0, `omphotom`
The purpose of `omphotom` is similar to that of `omsource`, namely to perform aperture photometry in OM images. There are two main differences between these tasks. `omphotom` offers a choice among several methods of computing the photometry. And it can be invoked as a line command

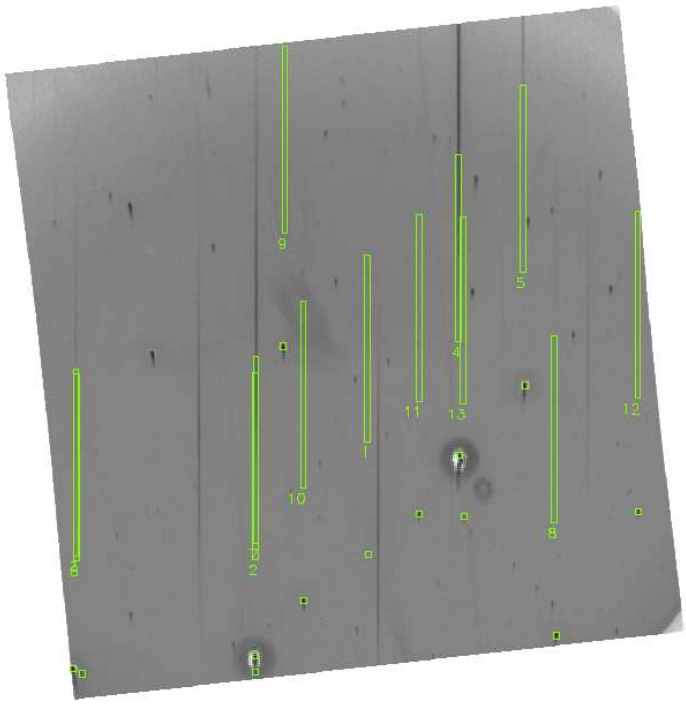

Figure 8: Detection of spectra obtained with the OM UV grism in the field of HD 13499 (the bright object on the mid-right part of the image)

e.g. to re-compute with the same parameters the photometry of a given source in a series of images.
The user is referred to the SAS on-line documentation for a detailed information on this new task.

6.4 Calibration items

6.4.1 Repeatibility of OM filter photometry

Several spectrophotometric standard stars (WD's) are observed repeatedly with OM in order to establish and monitor the photometric and flux calibrations. These are GD 153, HZ 2 and BPM 16274. All existing data of these stars have been reprocessed using SAS 8.0. The results are shown in Tab. 4. The errors are the standard deviation of the means given as percentage.
We see that after all corrections are applied, observations of standard stars taken along all the life of OM do not vary within 2 %.

6.4.2 Absolute fluxes: OM grisms and filters

As it has been explained in previous SAS validation reports, the OM has been calibrated in flux. This absolute calibration is based on observations of several standard stars obtained with filters and grisms. BPM 16274, a WD standard is observed evry 6 months to monitor the stability of OM, but it was not used to define the calibration.
In Fig.12 we show OM data of BPM 16274 compared with the reference spectrum of the star. The agreement between the OM elements processed with SAS and the comparison with the reference spectrum are excellent.

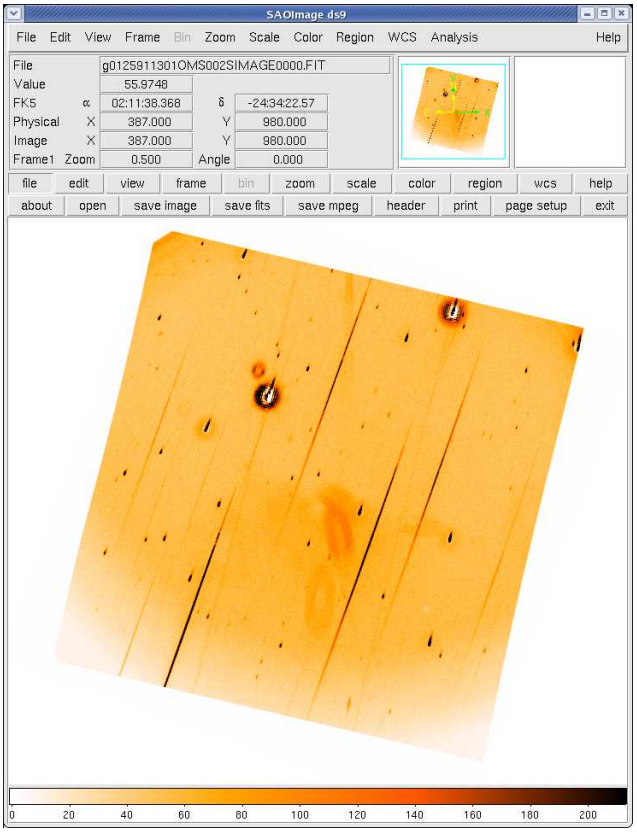

Figure 9: Sky aligned spectral image obtained with the OM UV grism in the field of HD 13499 (the bright object on the mid-right part of the image)

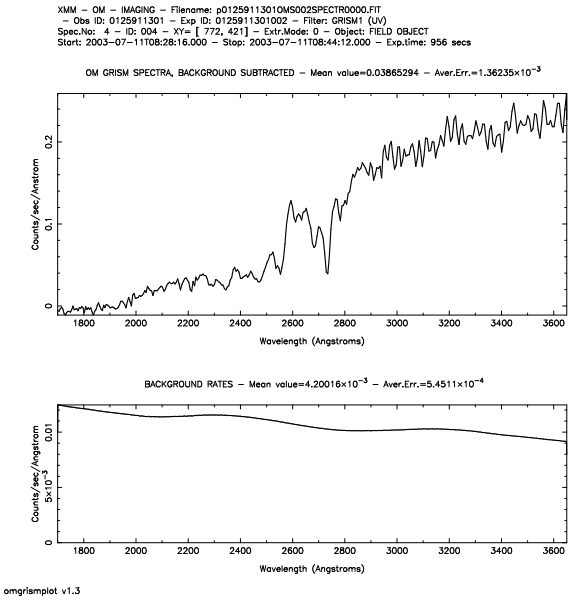

Figure 10: Extracted UV spectrum of HD 13499

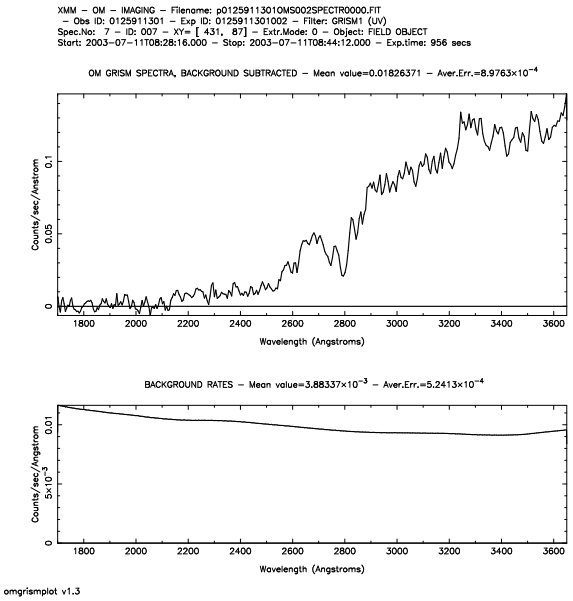

Figure 11: Extracted UV spectrum of HD 13434

Table 4: Standard stars: average count rates of several observations

star	N_obs	V	B	U	UVW1	UVM2	UVW2
GD153	8	81.81	160.25	326.87	417.80	282.64	70.45
error (%)		0.8	0.7	0.8	1.6	1.0	1.6
HZ2	8	23.28	47.50	110.70	168.61	148.35	43.12
error (%)		1.1	1.4	1.0	0.7	0.9	1.4
BPM16274	14	14.25	29.51	71.31	112.57	107.60	32.53
error (%)		2.0	2.8	1.7	0.9	1.3	1.3

6.5 OM Fast Mode

The time dependent sensitivity degradation correction, implemented for image photometry since SAS 6.5, has been included now also for fast mode processing. Therefore, light curves obtained at different epochs can now be compared. This is important, since for the UV filters the sensitivity has decreased about 10 % since launch (something less for the optical filters).

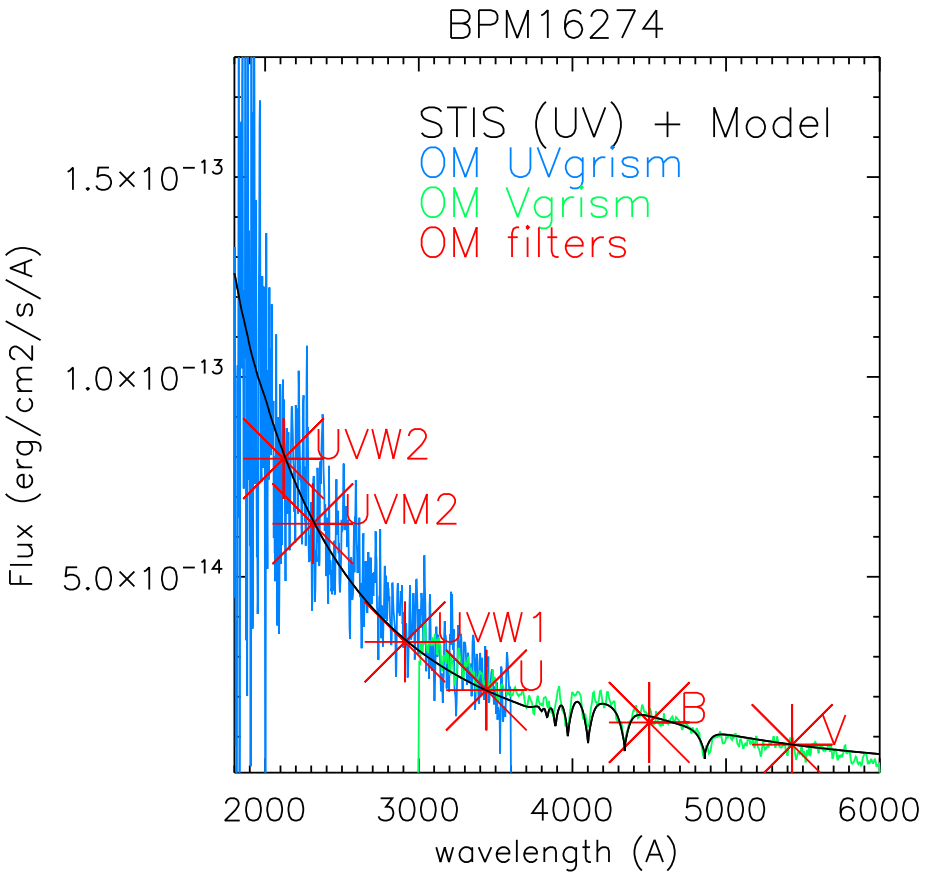

Figure 12: Fluxes of BPM 16274 obtained with OM filters and grisma compared with a reference spectrum of the star.

7 Results of new implementations

7.1 Light curves background subtraction and exposure correction tasks

The new task for exposure correction of EPIC light curves, `epiclccorr`, has been thoroughly tested. While final quantitative analysis of the data is still underway, based on the analysis of several Cataclysmic Variable observations and comparing with partly already published results, the qualitative analysis of background subtracted light curves in different exposure modes, has yielded so far very good results. Cross-checking has been performed not only with data from different EPIC cameras and modes, but also with exposure corrected RGS light curves using the task `rgslccorr` introduced in SAS 7.2, which so far had been only validated functionally.
A qualitative impression can be given by the results of correcting data from a bright cataclysmic variable, which shows a complex light curve structure. Data has been taken in different modes in this case with simultaneous exposures of MOS1 in Full Frame, MOS2 in Timing Mode and pn in Small Window Mode. We got at the same time spectroscopic data from RGS1 and RGS2. Fig. 13 shows the full corrected light curves of MOS1 and MOS2 in comparison, while in Fig. 14 we see a detail of this comparison. The analysis of the MOS1 data required a strong excise of the core of the PSF, due to pile-up. `epiclccorr` is able to correct for this. The average level of the correction is approximately 4 for MOS1 (of course this depends on how strongly the PSF core gets excised) and 1.3 for MOS2. No normalization has been applied to these data for the comparison.

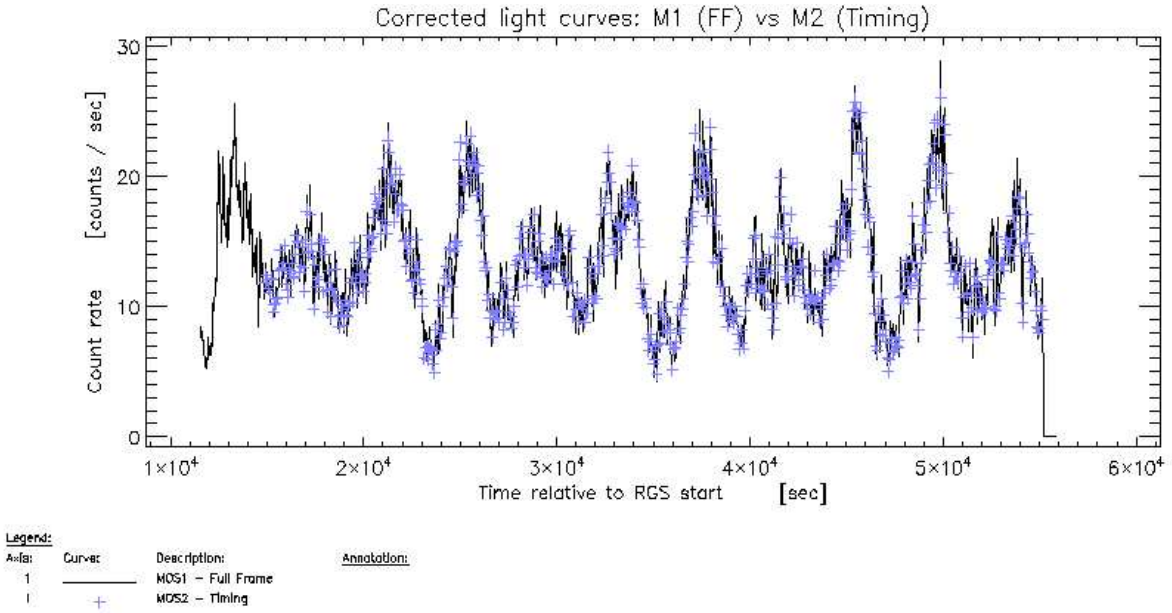

Figure 13: MOS1 vs MOS2 background subtracted and exposure corrected light curves

A normalization factor of 2 for MOS is needed in the case of the same comparison between MOS1 and PN, due to the different effective areas of the instruments, as shown in the corresponding Figs. 15 and 16[1].
The excellent correspondence of all the EPIC corrected light curves is also seen in the comparison with the RGS corrected light curves, as done by the task `rgslccorr`. In this case, however, small differences found should be attributed to the much more restricted energy range in the RGS

[1] Actually the factor is smaller than it should be. See further below for an explanation

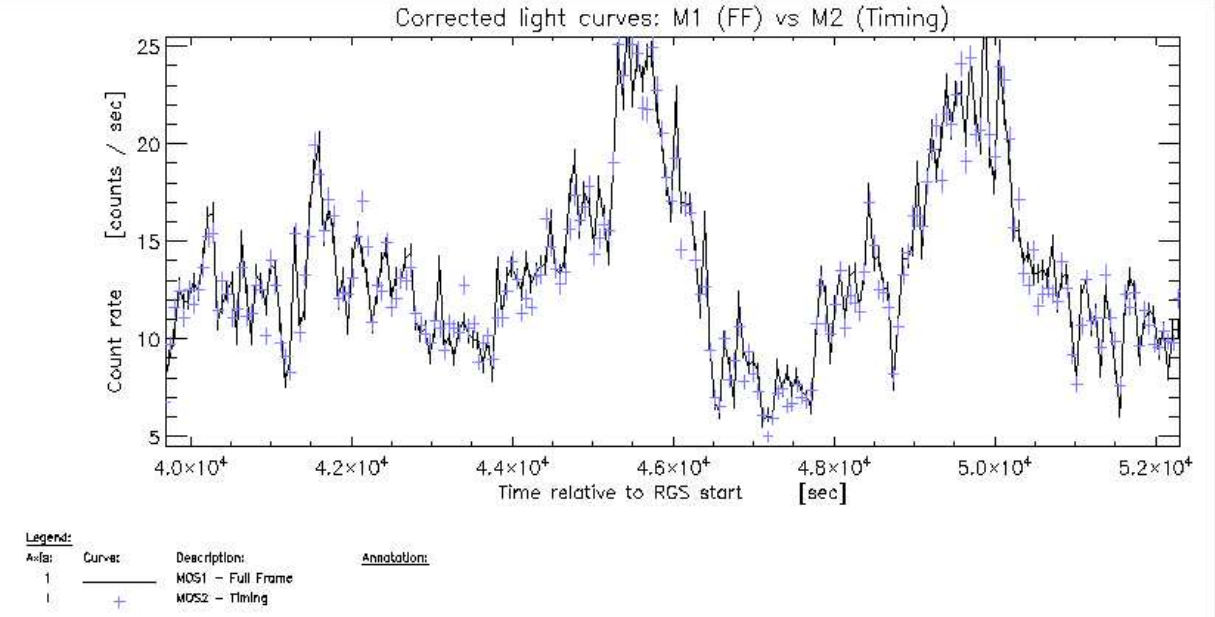

Figure 14: MOS1 vs MOS2 background subtracted and exposure corrected light curves - zoomed in

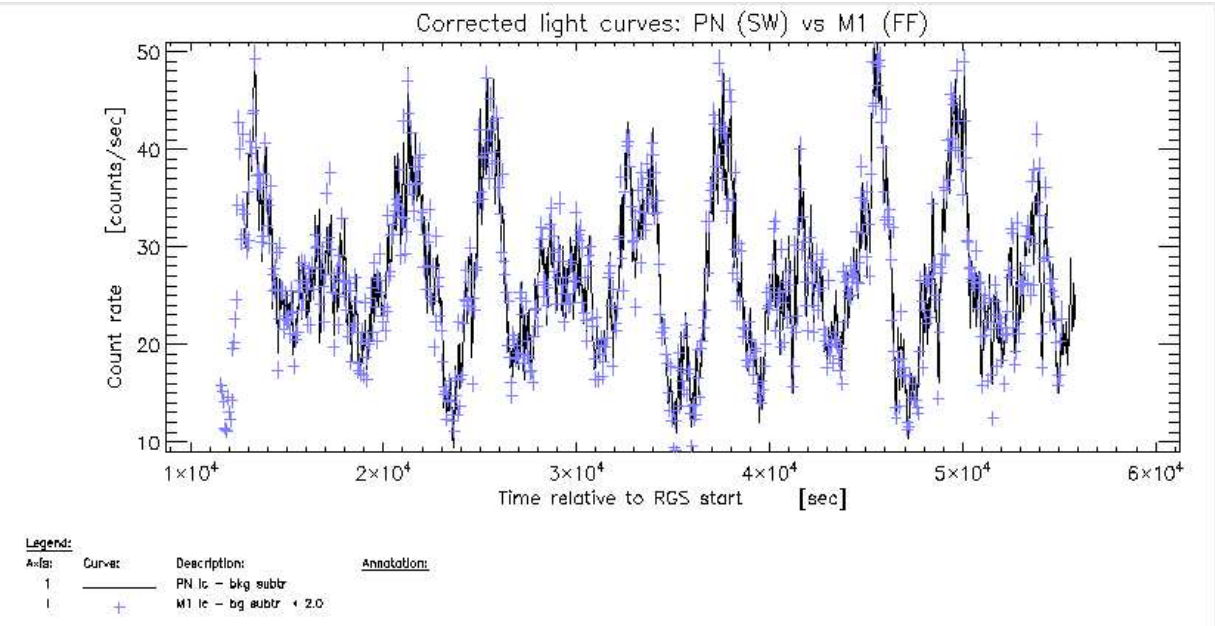

Figure 15: MOS1 vs PN background subtracted and exposure corrected light curves

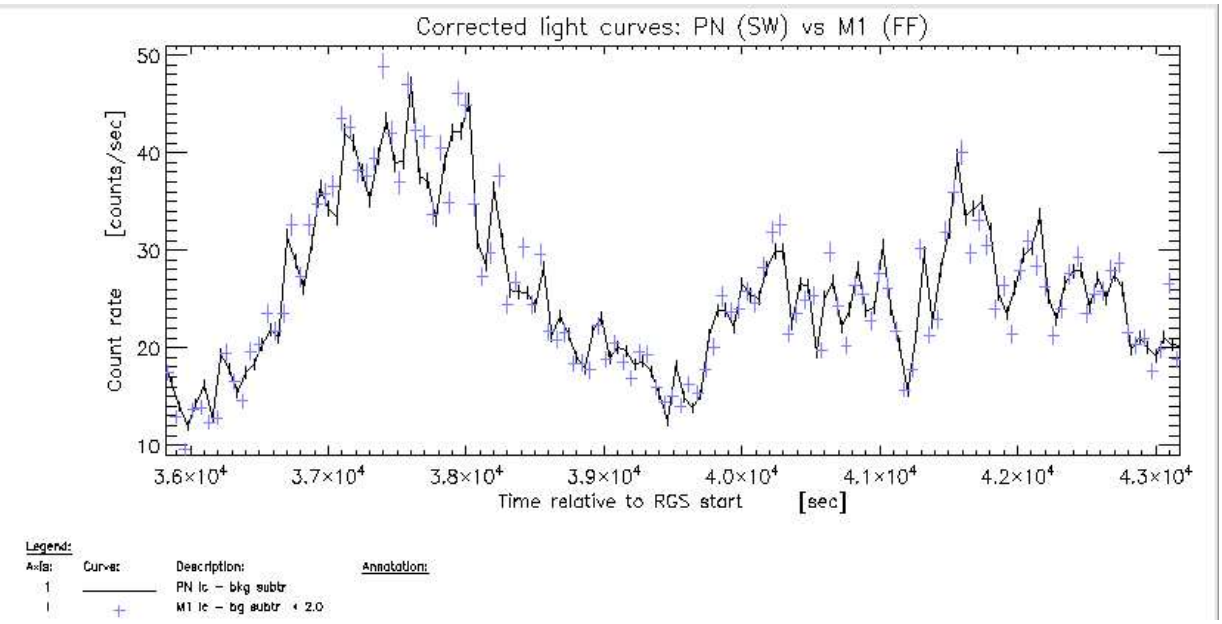

Figure 16: MOS1 vs PN background subtracted and exposure corrected light curves - zoomed in

analysis (E=[0.3-2.0]keV). Both RGS1 and RGS2 corrected light curves are compared in Figs. 17 and 18.
A quantitative analysis of these data and several other observations will follow. While qualitatively OK, some small problems have been found in a late validation stage, which make an upgrade release necessary (this is intended within a few weeks from the time of writing this report). We will wait, however, for the detailed analysis going on at the moment to be finished, before deciding when to proceed with such a sub-release. The problems found so far are:

- the readout time per frame is not properly taken into account for PN (due to the use of a wrong keyword), so that the dead times for reading out the CCDs are ignored. This introduces an absolute normalization error in an amount which is dependent on the observing mode. The count rates are underestimated as follows:
  - PN Timing mode: 1%
  - PN Extended Full Frame: 2%
  - PN Large Window: 5
  - PN Full Frame: 6%
  - PN Small Window: 30%
  - PN Burst Mode: 97%
- if the selection region for a source is distributed over 2 CCDs, running `epiclccorr` over it produces a seg fault, due to a bug in the handling of the memory.

This information has been included in a "watchout item" in the SAS web pages, to inform immediately the observers.

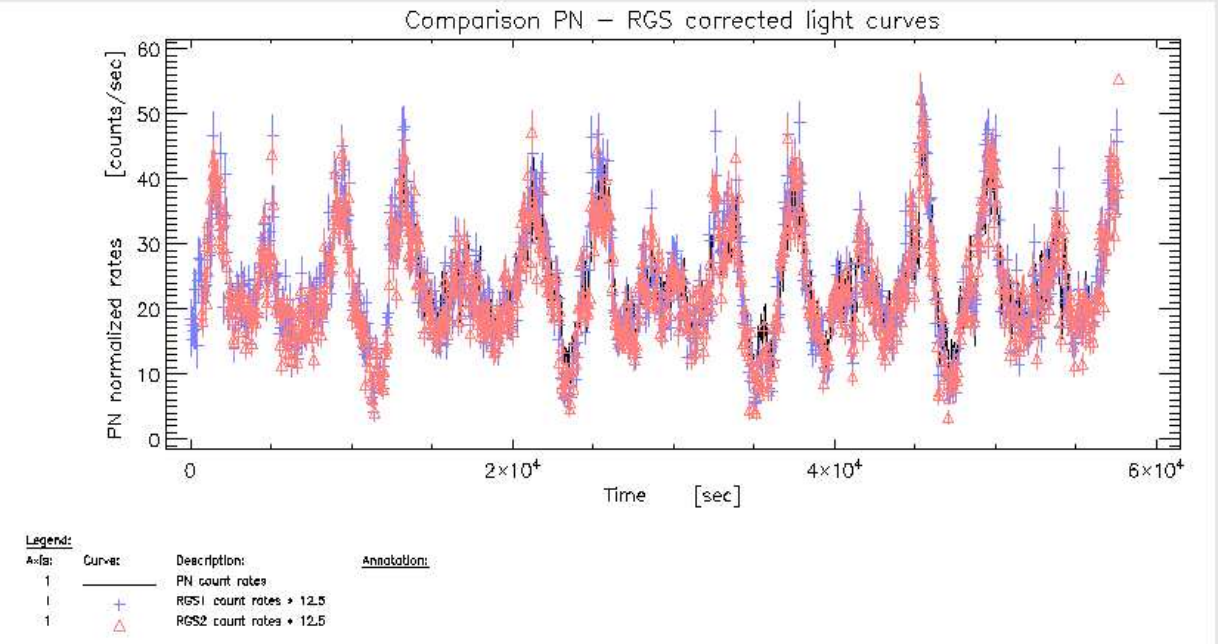

Figure 17: RGS vs PN background subtracted and exposure corrected light curves

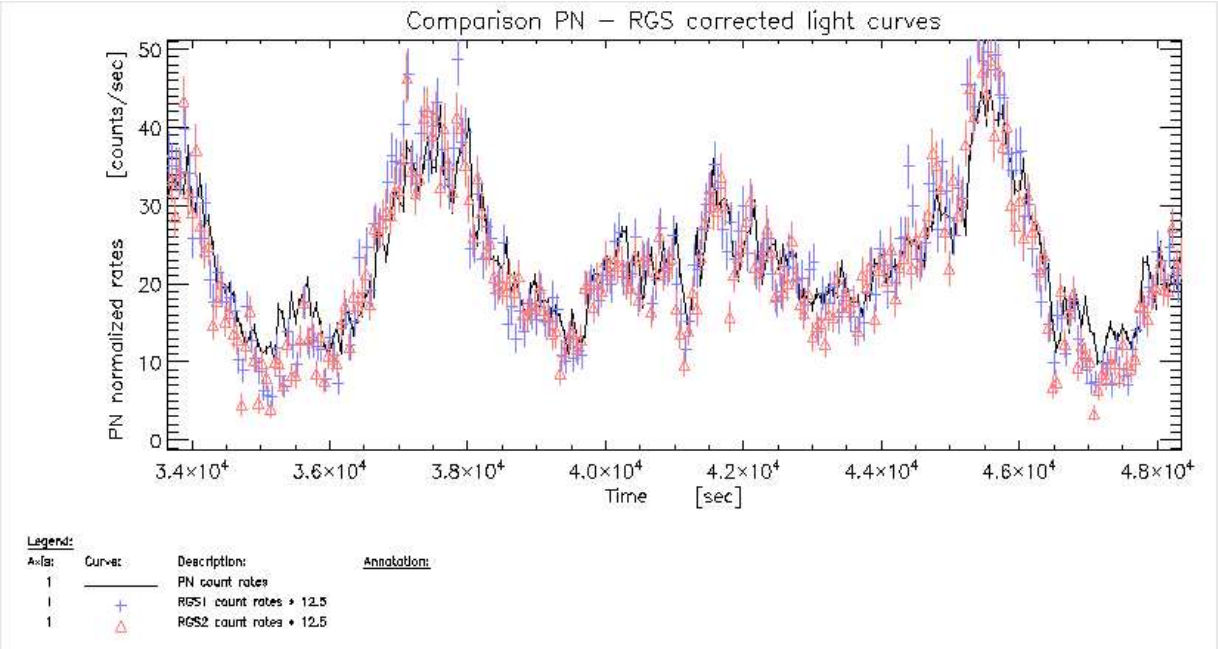

Figure 18: RGS vs PN background subtracted and exposure corrected light curves - zoomed in

7.1.1 Additional tests checking the performance of `rgslccorr`

The performance of the task rgslccorr has been tested in some observations with characteristics that make them particularly well suited for this purpose.
The test made was to generate light curves for both RGSs using the task `rgslccorr` and other methods, namely an IDL procedure and evselect. In the latter cases the proper scaling between the source and the background light curves was made using the keyword /PIX_ENCL/ present in the source and background extensions of the source list. In all cases the lightcurves generated with the IDL procedure and with evselect coincided, so we only refer the discussion to the first set. In the figures 19 to 21, the light curves obtained with `rgslccorr` (shown in black) are compared with light curves obtained with the IDL procedure (shown in red). IDL-generated light curves have been slightly shifted in time for a better display.

- Lockman hole (Obsid 0147511601):
No detectable signal in RGS. This dataset has been chosen to check if the scaling of the source and background region is done correctly, i.e. if the countrate of the background-subtracted light curve is zero. As shown in Fig. 19, the average count rate of the light curves obtained with `rgslccorr` for both RGSs is consistent with zero (0.003 ± 0.022 cts/sec for RGS1 and 0.008 ± 0.021 cts/sec for RGS2).

- RS Oph (Obsid 0410180301):
Due to the unexpectedly high brightness of the target, the allocated telemetry rates were not sufficient to handle the large event rate and all instruments were affected by telemetry saturation. The effective exposure times (as derived by e.g. `rgsspectrum`) were therefore shorter that the on-target time (9801 sec for RGS1 and 18640 sec for RGS2).
The difference in effective exposure time between both RGSs is mainly due to the lack of CCD4 in RGS2. This CCD covers the wavelength range 21-25 Å where the maximum of the emission occurs, and therefore the overall countrate in RGS2 is smaller than in RGS1, and the effect of the telemetry saturation is nearly negligible. The fraction of frames with lost events in RGS1 goes between 6% and 30%, depending on the CCD. RGS2 is less affected (there is a 2% of the frames with lost events in CCD6, in the rest the fraction being than 1%). Observed countrates in the first order extracted spectra are approximately 150 for RGS1 and 110 in RGS2. The problem of telemetry saturation obviously requires a careful treatment of the data to derive a correct RGS1 light curve.
Results are shown in Fig. 20, top RGS1 and bottom RGS2. For RGS2, where telemetry problems are minor, the agreement between the IDL and the SAS lightcurves is very good, except for a few bins. In the case of RGS1, the task has been able to re-construct the exposure in every bin and then to produce a correct light curve. The average countrate of the RGS1 lightcurve (163.91 cts/sec) matches well that of the extracted spectrum (162.33 cts/sec).

- Mkn 766 (Obsid 0096020101):
Fig. 21 shows the results obtained with the observation of this variable source, that shows variations over a wide range of time scales.

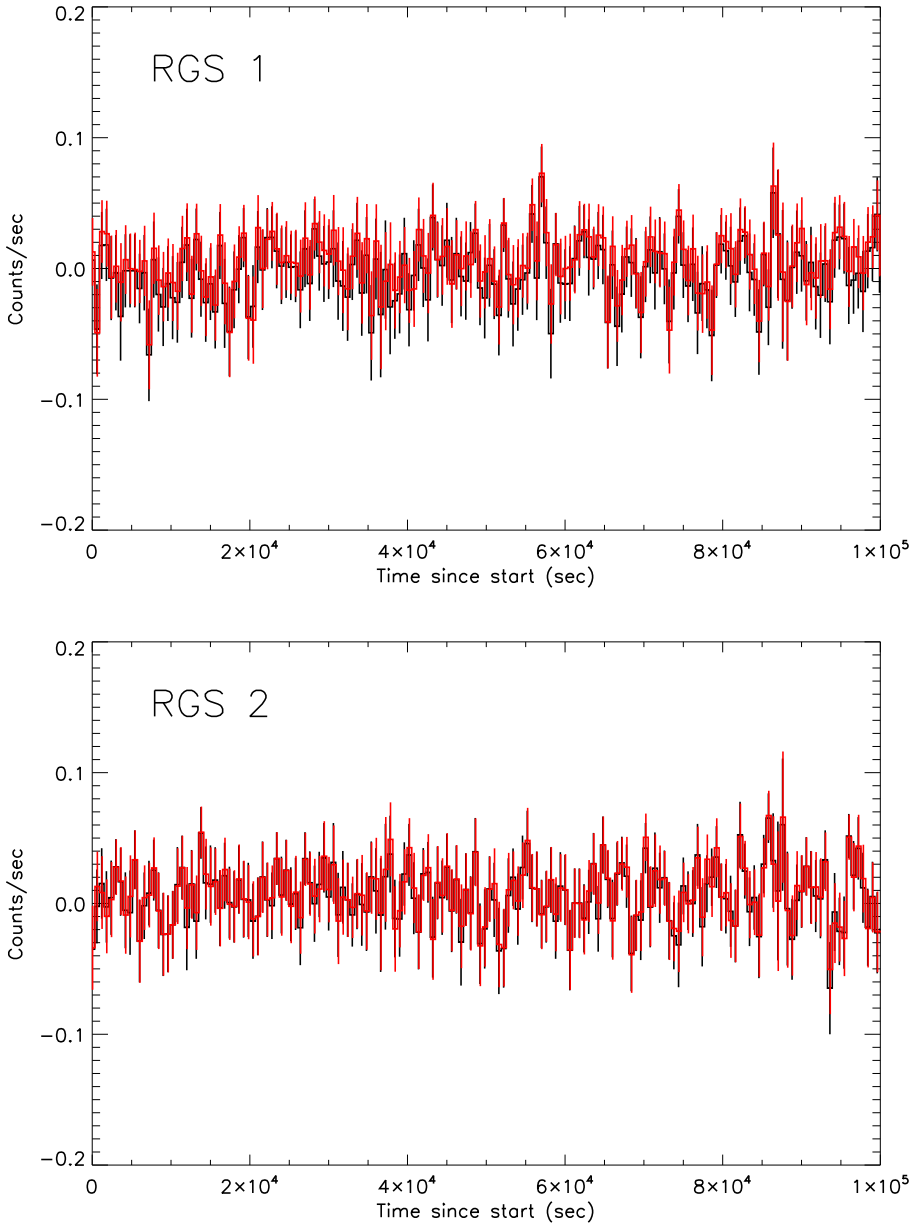

Figure 19: Comparison of RGS lightcurves for an observation of the Lockman Hole. Shown in black are the lightcurves derived with `rgslccorr` and in red those derived using an IDL procedure.

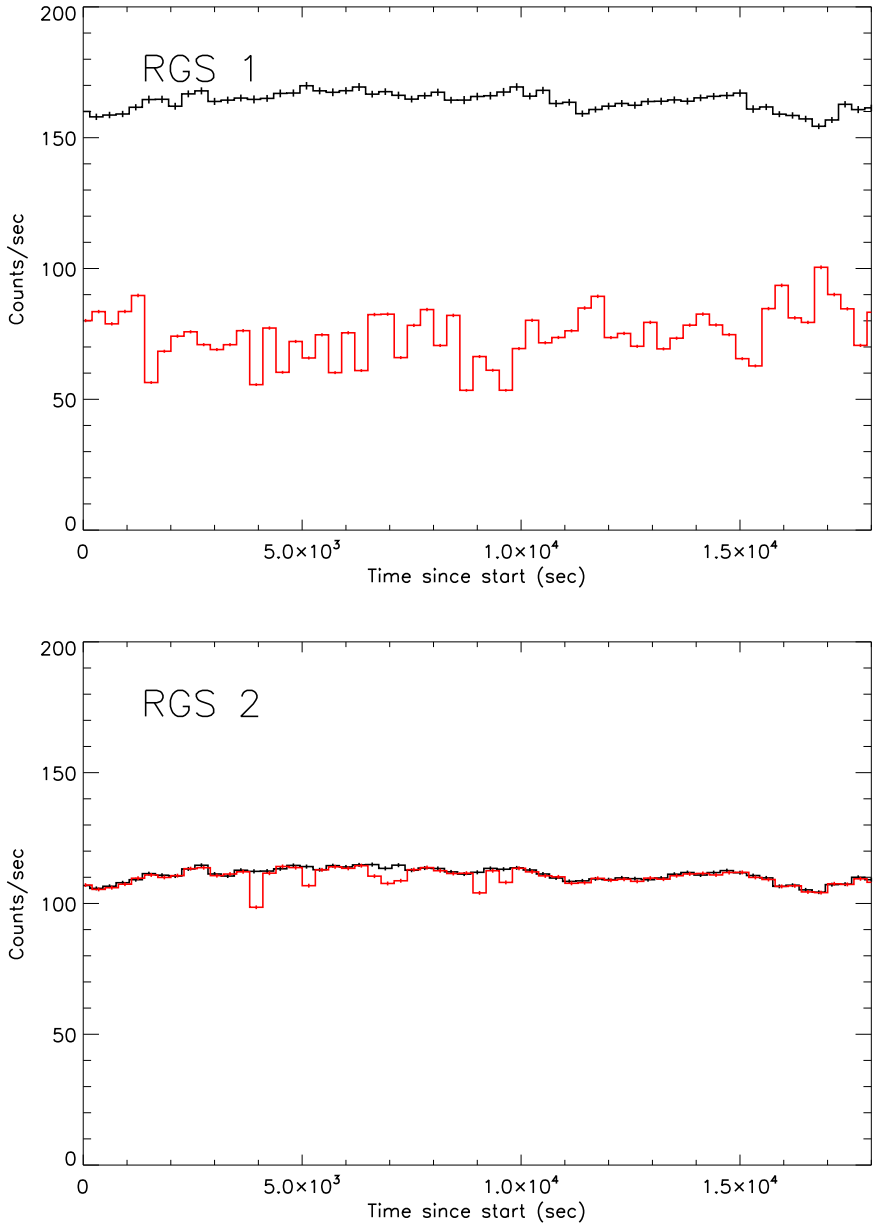

Figure 20: Comparison of RGS lightcurves for the observation of RS Oph of April 7 2006. Shown in black are the lightcurves derived with `rgslccorr` and in red those derived using an IDL procedure, that does not include any exposure correction.

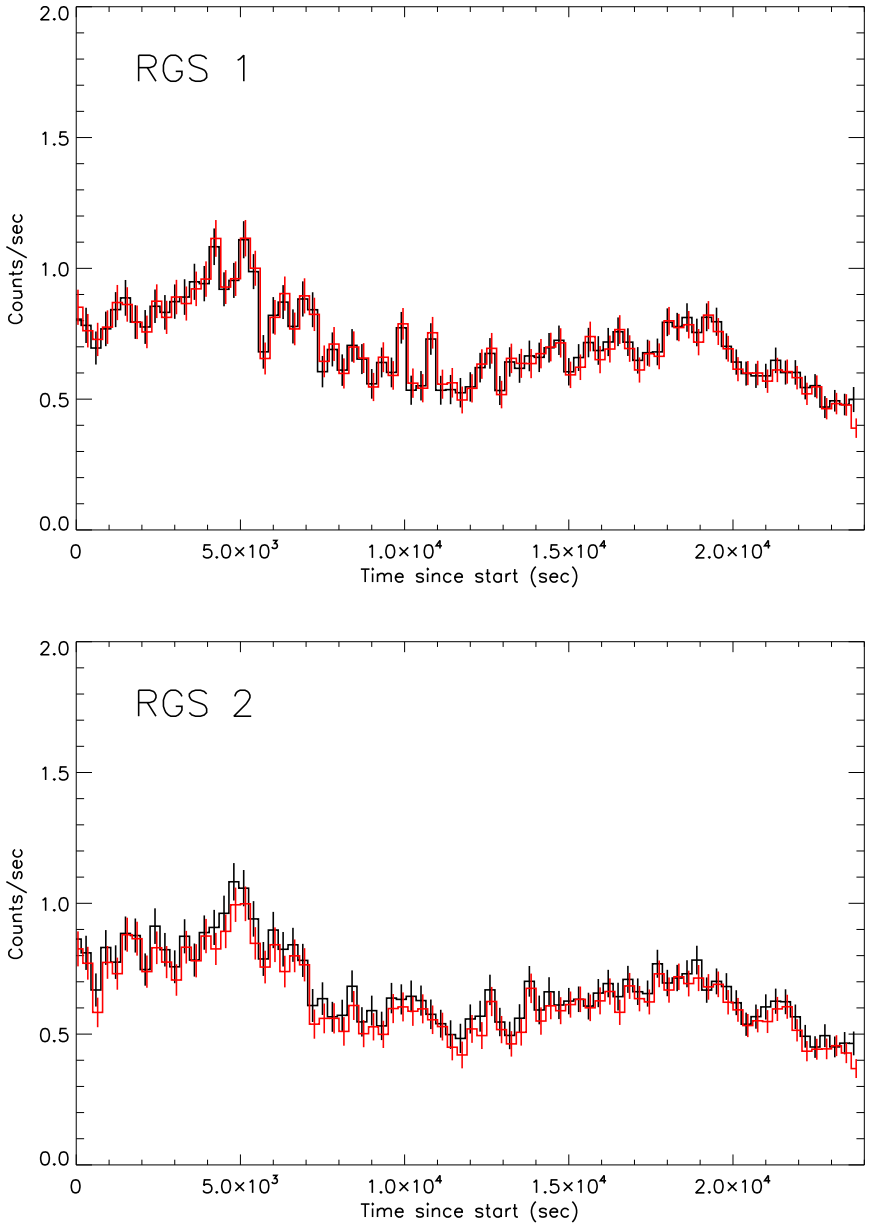

Figure 21: Comparison of RGS lightcurves for an observation of Mkn 766. Shown in black are the lightcurves derived with `rgslccorr` and in red those derived using an IDL procedure, that does not include any exposure correction. The slight difference in the absolute level of the light curves, in particular for RGS2, are most likely due to the different background/source scaling procedure.

7.2 `eslewchain`, the new task for slew data analysis in SAS

`eslewchain` is a SAS task for processing data taken during point-to-point spacecraft slews. It is available, for the first time, in the SAS 8 release.
`eslewchain` performs the basic processing of slew event data into a sequence of consecutive images (and exposure maps) along the slew path, each image being about 1 degrees by 1 degree. This process is a consolidation of the approach taken by dedicated software that has been used in the production of the XMM-Newton slew catalogue (XMMSL1[2]). Source detection on the images created by eslewchain images is performed separately using existing SAS tasks.
For this analysis, three Slew Data Files (SDFs) were used: 9099000003, 9145000003 and 9138800002.
The raw ODF data are preprocessed following the documentation, using `epproc` (with default parameters) to generate the input event list. Ensuring the SAS_ATTITUDE environment variable was set to RAF; the data were run through `eslewchain` to generate the images and exposure maps (29 images for 9099000003, 21 for 9145000003 and 56 for 9138800002).
A few images were compared with the corresponding images made for the slew catalogue. Simple subtraction was performed to check for consistency. For those tested, there was often an offset of 1 pixel (resulting in adjacent ± counts) but in random orientations, indicating that the deliberate spatial randomization used within the event file creation is the most likely cause. No systematic differences were seen.
To explore the results further, source detection was also performed on the images using a locally produced scripts based on the `edetect_chain` task. It should be noted that changes to `edetect_chain` (probably related to improvements made in `eboxdetect` for the detection of multiple sources) since SAS 6.1 yield more spurious detections - the slew catalogue is essentially based on processing using the SAS 6.1 version of `emldetect`. Here, however, the SAS 8 version of `emldetect` is used, along with the current public calibration files. The emergent `emldetect` source lists (one per image) were merged into one file and this was then cross-correlated with the (clean) slew catalogue using a 10" maximum correlation radius. This analysis was only conducted on the total (0.2-12 keV) (b0) band images (`eslewchain` generates images in this band and in the 0.2-2 keV (b4) and a 2-12 keV (b5) bands).
A total of 3 (9099000003), 5 (9145000003) and 9 (9138800002) detections from the SAS-8 `eslewchain` processing were matched to sources in the slew catalogue that had meaningful total band (b0) counts in the catalogue.
In terms of the astrometry, the offsets for the 3 matches in 9099000003 range from 1.4 to 3.9" (mean=2.4", not systematic). For 9145000003, the offsets range from 1.6" to 8" (mean offset = 4") - 4 out of the 5 matches have deviations < 4"). Here there is some evidence for the shift being systematic in RA. For 9138800002, the offsets vary from 1" to 10" (mean offset = 3.6") with all but one being <5" (six being <3").
Expressed as a fraction of those measured in the slew catalogue, the measured source counts deviate by up to 16% (mean deviation = 5%) for 9099000003. the DETML values are broadly in agreement. For 9145000003, the largest deviation is 17% with a mean of zero. DETML values are again reasonably consistent. In the case of 9138800002, the maximum deviation is 37% (mean deviation = -5%) with seven cases below ∼15%. Again, there is generally good agreement for the DETML values.
Overall, given the essentially unavoidable differences in the software (and calibration) used between this processing and that used for the slew catalogue, it appears that both the astrometry and photometry resulting of sources from source detection of images produced by eslewchain are within acceptable limits compared to the slew catalogue.

[2]R.D. Saxton, A.M. Read, P. Esquej, M.J. Freyberg, B. Altieri, D. Bermejo, 2008, A&A 480, 611

7.3 Source detection, astrometry and flux comparisons with 2XMM

The single Lockman hole observation (0147511601) has been used to compare the detection of sources and their astrometry and photometry with measurements derived from the SAS used in making the 2XMM catalogue. The observation was made with the MOS1, MOS2 and PN instruments in full frame mode with the Medium filter.
MOS and PN event files were produced using the `emproc` and `epproc` scripts with default parameters. Standard XMM-Newton multi-band (1–5) images were subsequently created after filtering out background flaring events. These images were then passed through `edetect_chain` using the default parameters, except that the ecf parameter was set to use the ECF values that pertained for 2XMM. The emergent source list was run through `eposcorr` and `srcmatch` and then cross-correlated with the corresponding list from the 2XMM processing.
We should note that there are significant differences here, both in the apparent cut of events which resulted in lower event numbers in the images compared to those from the 2XMM processing and in the parameters used with the detection chain (which resulted in a higher likelihood threshold being applied).

7.3.1 Source detections:

We hereafter are concentrating on the sources detected with EP_DET_ML$\geq$ 10 with SAS 8, the number of which is 178. The vast majority of these 178 sources are also detected in the 2XMM processing, the majority of which have EP_DET_ML$>$ 10 in the 2XMM processing as well. After the source matching between those two, namely the source list with SAS 8 and 2XMM, based on the angular distance between them (3 arcsec at maximum), 160 sources were found to be common.
Fig. 22 shows the spatial distributions of the sources detected with SAS 8 and 2XMM. It seems that SAS 8 sometimes picks up more than one source close to each other in crowded regions, where the 2XMM picks up just one source. On the other hand, some of the sources detected in the 2XMM are missed in SAS 8. This can be explained with the fact that the SAS 8 processing here resulted in lower event number, as mentioned above (Sec 7.3).
Now we filter out the extended sources based on `EP_EXTENT`, and are concentrating only on the point-like sources, the number of which is 155 out of 160 matched sources.
The next important parameter is the maximum likelihood (`DET_ML`) in the source detection. Fig. 23 shows the relation between the SAS 8 and 2XMM processing. They agree with each other well overall. In a small number of cases, particularly in low likelihoods, the 2XMM results show somewhat higher likelihood values. Again this can be explained with the fact that the SAS 8 processing here resulted in lower event number, as mentioned above (Sec 7.3).

7.3.2 Astrometry:

Fig. 24 shows the difference in the celestial coordinates between SAS 8 and 2XMM processing. The majority of them coincide with the accuracy of $\pm$0.5 arcsec.

7.3.3 Flux:

Figs. 25 and 26 show the differences in fluxes with each detector and energy bands between SAS 8 and 2XMM results. Overall they agree with each other reasonably well.
There is a trend that 2XMM fluxes are slightly higher particularly for the lower flux sources. Again this can be explained with the fact that the SAS 8 processing here resulted in lower event number, as mentioned above (Sec 7.3).

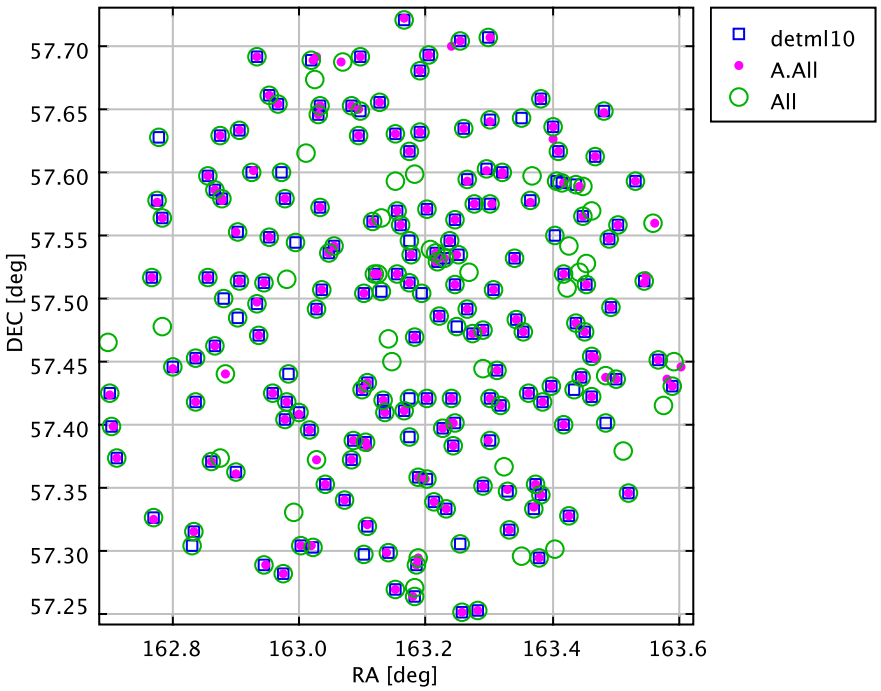

Figure 22: The position of the detected sources. The filled magenta circles and open blue squares are for the sources with EP_DET_ML≥ 10, detected with SAS 8 and 2XMM, respectively, whereas the green open circles are with $EP\_DET\_ML \geq 6$ from 2XMM.

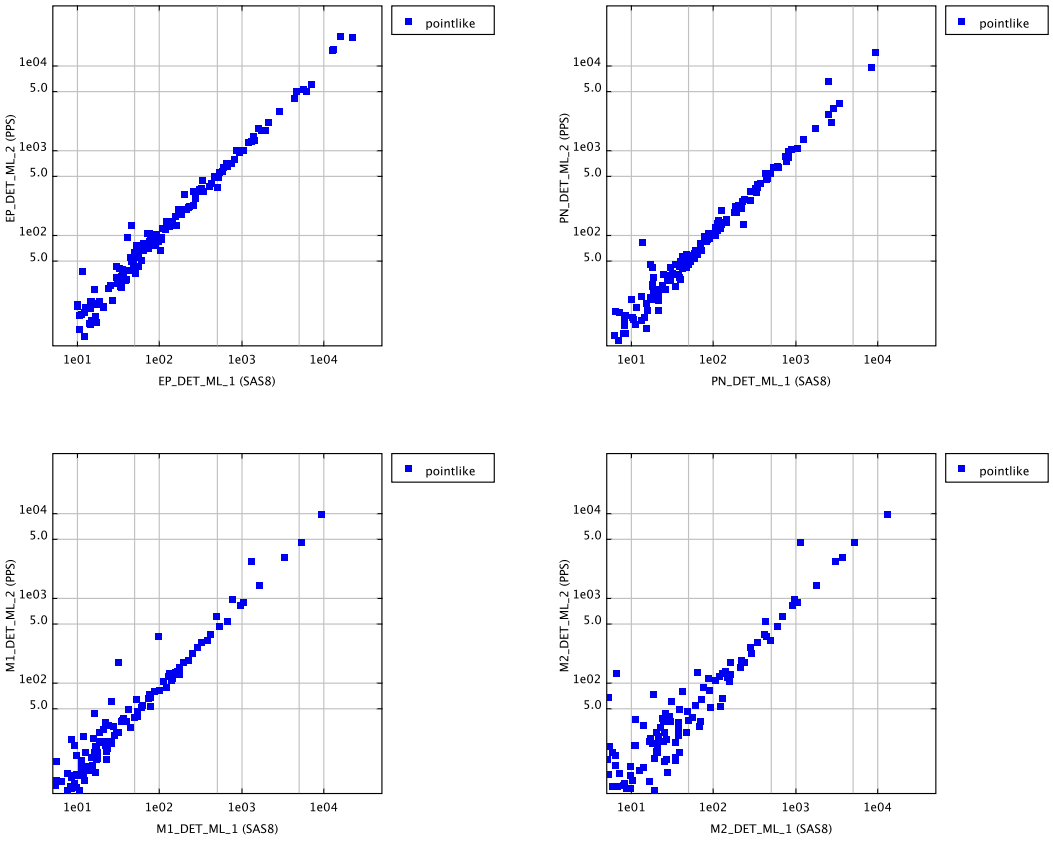

Figure 23: Difference in the maximum likelihood (`**_DET_ML`). The X and Y-axes are for the SAS 8 and 2XMM processing, respectively. From top-left panel to right, they are with all EPIC, pn, MOS1 and MOS2.

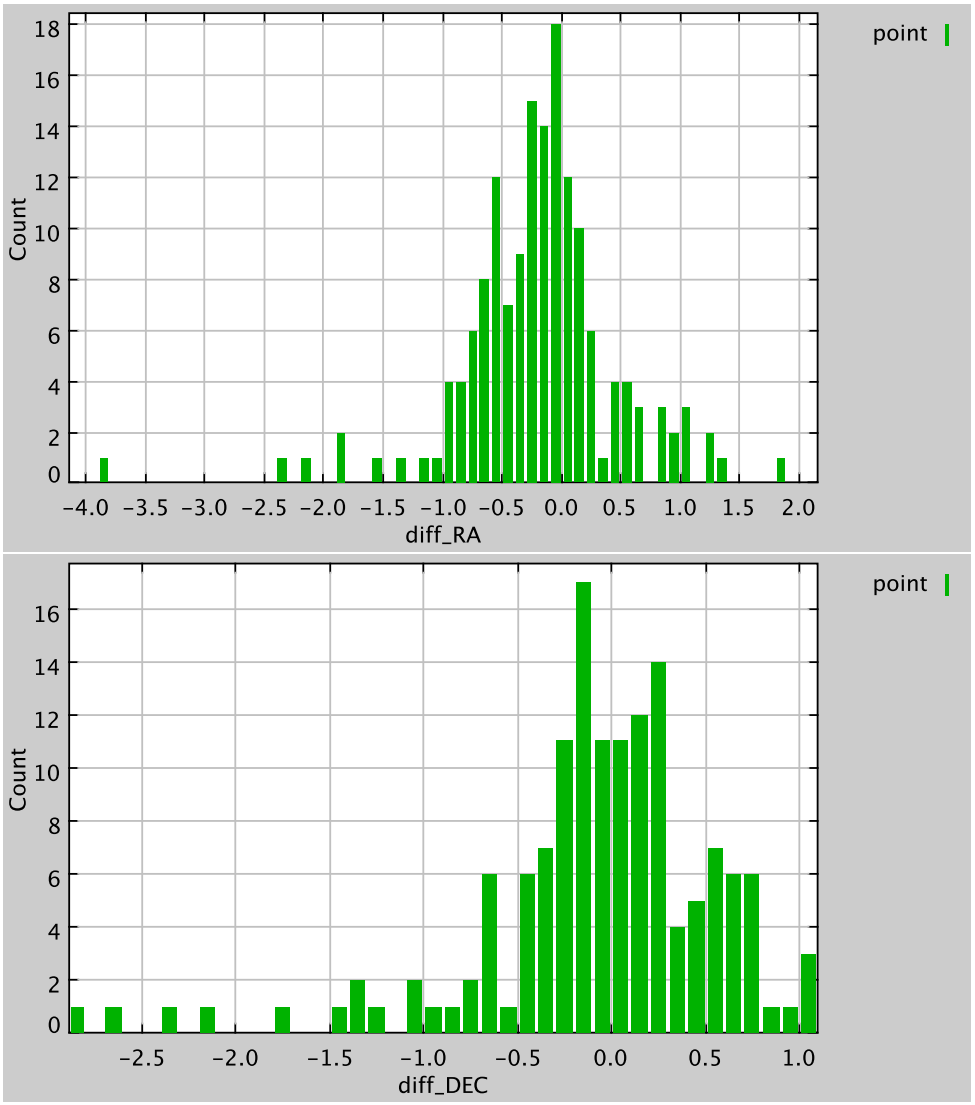

Figure 24: Difference in the celestial coordinates in unit of arcsec between SAS 8 and the 2XMM processing. *Top panel*: R.A. *Bottom panel*: Dec.

We found the scatter is marginally larger for MOSs than pn. It is possibly because of the lower statistics in MOSs than pn.

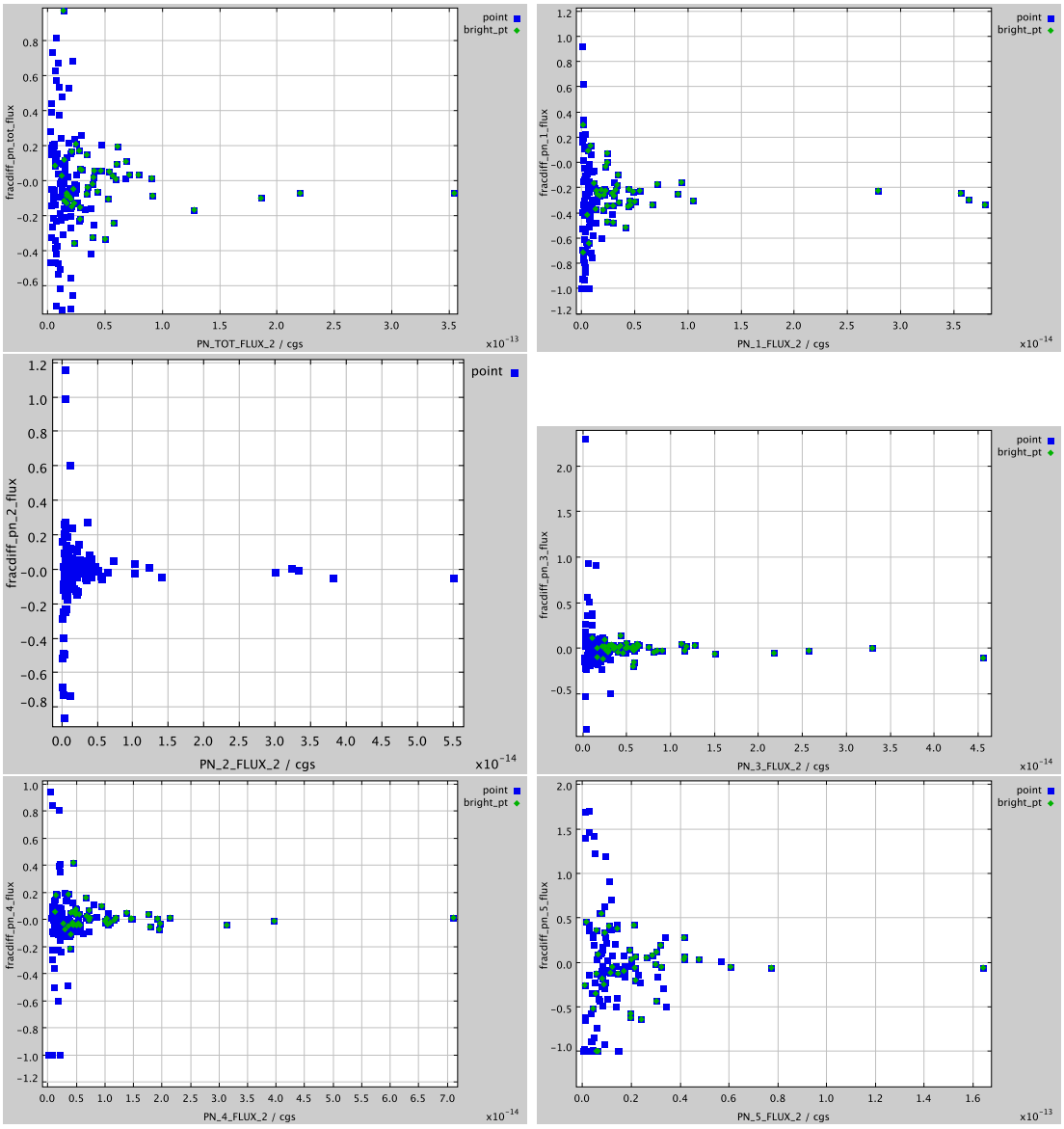

Figure 25: The ratio of the difference between the SAS 8 and 2XMM fluxes with pn to the corresponding 2XMM flux. From the top-left panel to right, they are for the total band and band 1 to 5, respectively.

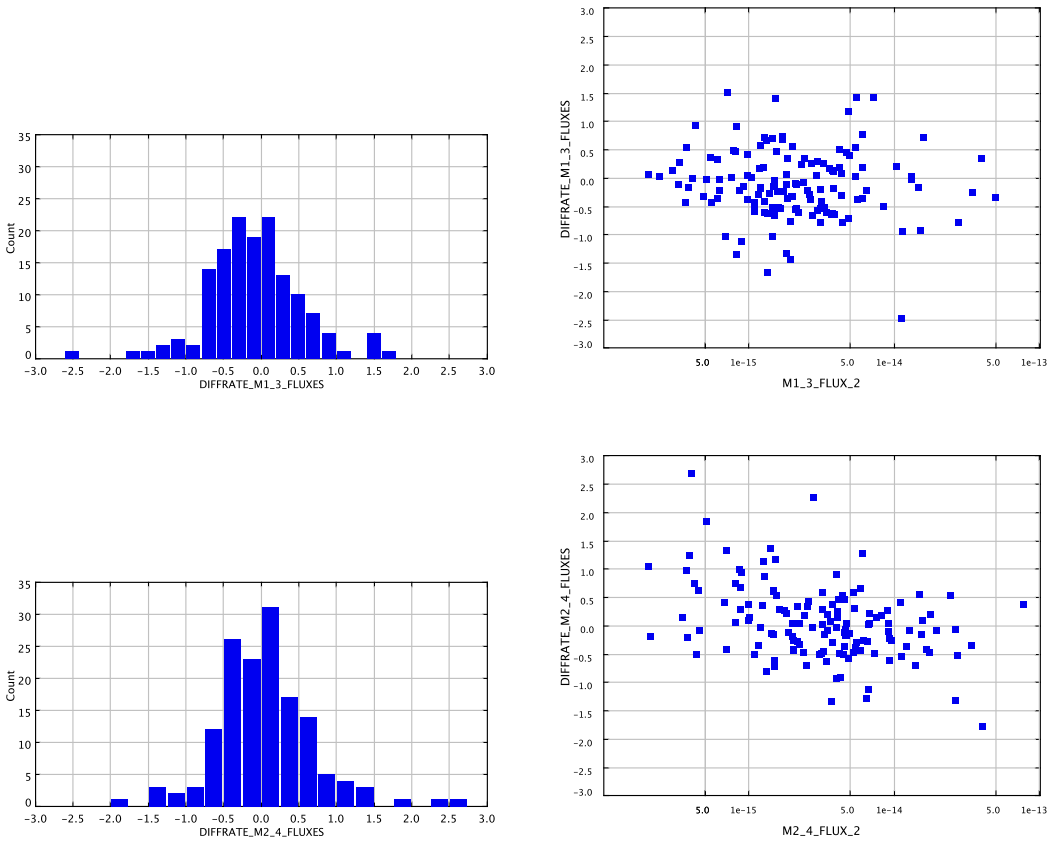

Figure 26: The ratio of the difference between the SAS 8 and 2XMM fluxes with MOS1 (*Top panels*) and MOS2 (*Bottom panels*) to the corresponding 2XMM flux. 90 and 88 per cent of the sources fall into the range of -1 and $+1$ for MOS1 and 2, respectively.

7.4 Updates implemented requiring still calibration

`epfast`, the new task for CTI and gain correction of PN fast modes, and the upgrades of `eregionanalyse`, `arfgen` and `xmmselect`, which implement the parameterisation of a 2D PSF as an ellipse, conclude in s/w terms a lot of efforts of the EPIC team for improving the calibration in these two areas. However, and given the wide parameter space involved in both cases, calibration could not be finished in time for the SAS 8 release. Thanks to the dynamic of the XMM-Newton calibration concept, however, as soon as the calibration is considered mature and the individual calibration files (CCFs) involved are released, they will be made public and so the upgrades will be fully operational. For this validation, only functional tests have been conducted, which were completely succesful.

7.5 "Time Jumps" in PN data

The new strategy for detection of "time jumps" (eg. inconsistencies in the flow of photon arrivals) in the PN data has been confirmed as succesfully implemented in SAS 8.0. The number of exposures affected by residual uncorrected time jumps is reduced from 15.6% (pre-SAS 8) to 2.2%.

8 Conclusions

The main conclusion of the SASv8.0 SV exercise can be summarized as follows:

- SAS 8.0 can reduce data taken with all the EPIC, OM, and RGS scientific observation modes,
- it incorporates the ability to process the EPIC data taken during slews between observations pointings through a new task `eslewchain`,
- SAS 8.0 offers a new task (`epiclccorr`) for background subtraction and exposure correction of light curves from any EPIC mode,
- the times for reading out the EPIC PN CCDs, however, have not been taken into account, so that the absolute level of the corrected light curves is affected. This will be fixed in a patch release of `epiclccorr` very soon,
- the `epiclccorr` patch will also solved the problem found with sources distributed on different CCDs, which at the moment cannot be properly processed by the task, due to a bug,
- `epiclccorr` has helped to validate the task released with the former SAS version, `rglslccorr`, performing light curve exposure correction and background subtraction for RGS data,
- the quality of EPIC and RGS spectral fitting is slightly improved, and residuals in the simultaneous spectral fitting of all X-ray instruments slightly reduced, (details in the corresponding calibration status documents under http://xmm2.esac.esa.int/external/xmm_sw_cal/calib/),
- SAS 8.0 includes the alternative RGS data reduction using a grid of wavelength bins, making possible the rigorous combination of spectra from several observations,
- a new strategy against "Time Jumps" in the EPIC PN data has been succesfully implemented, which reduces considerably the number of exposures affected by residual uncorrected occurrences,
- a new task for EPIC PN fast modes rate dependent CTI and gain correction has been implemented (still lacking final calibration),
- as well as a new parameterisation of a 2D PSF as an ellipse for a better characterization of encircled energies of EPIC offset sources. This is also waiting for final calibration numbers, which is expected soon,
- SAS 8.0 offers a more robust and accurate interactive extraction of OM Grism spectra,
- an alternative task for performing OM photometry is offered in this version, `omphotom`, implementing diverse photometry methods,
- SAS 8.0 OM software includes time dependent sensitivity correction for fast mode, and therefore the possibility of comparing light curves obtained at different epochs.

Table 5: XMM-Newton instrument scientific modes supported by the SAS and the PPS

Mode	Processed by SAS?	Processed by PPS?
	MOS	
Full Frame	Y	Y
Large Window	Y	Y
Small Window	Y	Y
Timing Uncompressed	Y	Y
Slew Data	Y	N
	pn	
Full Frame	Y	Y
Extended Full Frame	Y	Y
Large Window	Y	Y
Small Window	Y	Y
Fast Timing	Y	Y
Fast Burst	Y	Y
Slew Data	Y	N
	RGS	
Spectroscopy	Y	Y
	OM	
Image Mode	Y	Y
Fast Mode	Y	Y
Full Frame Low Resolution	Y	Y
Full Frame High Resolution	Y	Y
Science User Defined	Y	Y

Appendix A: Matrix of supported instrument modes by SAS v8.0

In Tab. 5 we show the list of science instrument modes which can be processed by the SAS, and are currently being routinely processed by the pipeline.